Synthesis and characterization of magnetic adsorbent prepared by magnetite nanoparticles and zeolite from coal fly ash

Mitiko Yamaura & Denise Alves Fungaro

Journal of Materials Science
Full Set - Includes `Journal of Materials Science Letters'

ISSN 0022-2461
Volume 48
Number 14

J Mater Sci (2013) 48:5093-5101
DOI 10.1007/s10853-013-7297-6

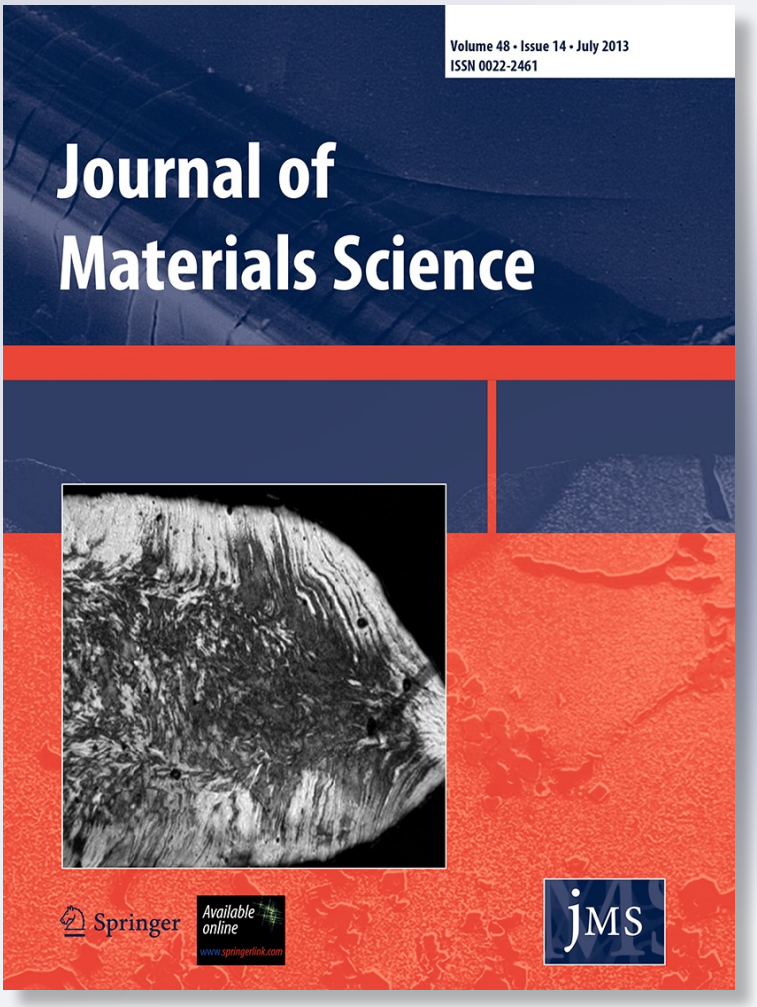

Springer

J Mater Sci (2013) 48:5093–5101
DOI 10.1007/s10853-013-7297-6

Synthesis and characterization of magnetic adsorbent prepared by magnetite nanoparticles and zeolite from coal fly ash

Mitiko Yamaura · Denise Alves Fungaro

Received: 12 December 2012 / Accepted: 6 March 2013 / Published online: 2 April 2013

Abstract Magnetite nanoparticles were prepared by partial oxidation of Fe(II) ions of an aqueous suspension of hydroxysulfate green rust which was obtained by precipitation of Fe(II) ions. This magnetite was mixed with zeolite synthesized from coal fly ash to obtain the magnetic adsorbent and the final product characterization was made. By analysis of scanning electron microscopy and X-ray diffraction, images of clusters of magnetite nanoparticles were observed and crystallite sizes of 17 nm were determined, respectively. In thermal analysis, the weight ratio of 1:3 for magnetite-zeolite in the magnetic adsorbent was measured and a non-magnetic product at 974 °C was found in both magnetite and magnetic adsorbent. Magnetization measurements described small hysteresis from the clusters of magnetite nanoparticles. Fourier Transform Infrared spectroscopy analysis indicated that the synthesized zeolite is a hydroxy sodalite and evidences of formation of the magnetic adsorbent were observed. The performance of magnetic separation technique was evaluated and it was comparable to the centrifugation process. The magnetic adsorbent indicated a potential application for adsorption of dye Reactive Orange 16 from aqueous solution.

Introduction

Magnetic adsorbents have been developed as an alternative technology of wastewater treatment. It is a known technology in biological assays as magnetic carriers that can be successfully employed in removing contaminants. Magnetic carriers have binding sites for biological molecules and present magnetic properties. Among other phenomena, the binding with the molecules can occur by adsorption. The combination of these two properties, adsorption and magnetic, into one composite allows obtaining a magnetic adsorbent potentially applicable in the wastewater treatment. This composite can be used to adsorb contaminants and subsequently can be removed from the medium by a magnetic separation method using an external magnetic field [1] and without the use the filtration or centrifugation.

Many authors have documented the technology of magnetic adsorbents by incorporation of magnetic nanoparticles of iron oxide on adsorbent substrates. Magnetite (Fe_3O_4) and maghemite (γ-Fe_2O_3) are the most commonly employed. Magnetic adsorbents where the core is a cluster of magnetic nanoparticles do not retain remanent magnetization; so that, with the removal of the external magnetic field they can be resuspended in another liquid medium. This property allows to conduct adsorption/desorption processes on magnetic adsorbent, and its reuse. It is a technology relatively simple without generation of secondary effluents.

The adsorbent substrates of the magnetic adsorbents [2, 3] can be natural or synthetic materials which have shown efficiency in removing dyes and metal ions [4, 5]. Zeolites are effective adsorbents and can be used to remove dangerous heavy metals from effluent streams [6, 7].

Natural zeolites have been combined with nanoparticles of maghemite and goethite to form magnetic zeolites for Cu(II), Cr(III), and Zn(II) as investigated by Oliveira et al. [8]. Other works about magnetic zeolites are found in the literature [9–11].

M. Yamaura (✉) · D. A. Fungaro
Chemical and Environmental Center, Nuclear and Energy Research Institute (IPEN-CNEN/SP), Avenue Prof. Lineu Prestes 2242, São Paulo CEP 05508-000, Brazil
e-mail: myamaura@ipen.br

D. A. Fungaro
e-mail: dfungaro@ipen.br

A solid waste of large volume from industrial activities is the coal ash produced by coal-fired power plants. This sub-product is usually disposed of in uncontrolled coal waste disposal sites or landfills that can lead to risk of serious contamination of soil, groundwater, and surface water with arsenic and other heavy metals [12, 13]. Studies indicate a high feasibility of using coal ash as building materials [14–16] and as fertilizers in agriculture [17]. Another form of its recycling is the obtaining of synthetic zeolites. The coal ash is composed mainly of silica and alumina and, therefore, can be converted into zeolites by hydrothermal treatment with alkaline solutions [18–20].

Zeolites from coal ash have been prominent as adsorbents for metal ions and dyes in liquid medium [21–23]; however, they are an ultrafine powder and it makes the process of solid–liquid separation harder. After the adsorption of metal ions or dyes, the filtration or centrifugation used in the stage of zeolite-supernatant separation is onerous. On the other hand, zeolite powder with magnetic properties can be easily removed by the technique of magnetic separation. The zeolite magnetic powder can be attracted and agglomerated with a magnet and the supernatant can be discarded. The magnetic separation technique combined with adsorption makes the wastewater treatment process simpler than applying a centrifugation or filtration.

In this work, magnetite particles were synthesized by precipitation and partial oxidation of Fe(II) ions in an alkaline medium and were combined with the zeolite from coal ash to form the magnetic adsorbent. These materials were characterized, and the performance of the techniques of adsorption of dyes Reactive Orange 16 and magnetic separation on magnetic adsorbent was evaluated.

Experimental

All chemicals used were of analytical grade. Reactive Orange 16 (RO16; C.I. 17757; $C_{20}H_{17}N_3O_{11}S_3Na_2$; molar mass = 601.54 g·mol^{-1}) was purchased from Sigma-Aldrich (50 % purity). The sample of coal fly ash from baghouse filter was obtained from a coal-fired power plant located at Figueira City, in Parana State, Brazil. All experiments were performed at room temperature (25 ± 2 °C).

Zeolite synthesis

Coal fly ash was used for zeolite synthesis by hydrothermal treatment where 20 g of fly ash was mixed with 160 mL of 3.5 mol L^{-1} NaOH solution and heated to 100 °C in an oven for 24 h. The zeolitic material product was repeatedly washed with deionized water and dried at 100 °C for 24 h [24]. This product was called SZ.

Magnetite particles synthesis

Magnetite particles were obtained by the method of precipitation and partial oxidation of Fe(II) ions. A solution of ferrous sulfate containing 0.0651 mol L^{-1} was prepared by dissolution of $FeSO_4{\cdot}7H_2O$ salt in 100 mL of distilled water. Aliquots of 0.250 mL of the solution of 2.5 mol L^{-1} NaOH were added progressively at time intervals of 30 s into the ferrous sulfate solution under stirring at 8,000 rpm using a Quimis disperser, model Q252K28, until obtaining the pH 11 at room temperature. Dark green precipitates with gelatinous aspect were formed. Variations of pH of the ferrous sulfate solution were recorded as function of the volume of added NaOH. After reaching pH 11 the addition of NaOH was stopped and the stirring was kept for 10 min which ensured the homogeneity of the suspension and the aerial stirring. Then the suspension containing dark green gel-like precipitate was boiled in a water bath for 75 min to complete the formation of a black precipitate. The dark green precipitate turned into a black, dense, and magnetic precipitate known as magnetite. The supernatant solution was discarded and the precipitate was washed several times with distilled water using the magnetic separation technique to sedimentation of the magnetic black solid phase and for the removal of wash water. After the washing, the wet solid phase was divided in two parts. One part of black solid was dried at room temperature to obtain a powder which was called MAG. Another was used immediately to prepare the magnetic adsorbent.

Magnetic adsorbent

The wet magnetite particles obtained according to the described procedure were used to prepare the magnetic adsorbent. A quantity (0.5 g) was suspended in 40 mL of distilled water and 1.5 g of SZ was slowly added into it under agitation. The used SZ/magnetite ratio was 3:1 (w/w). The obtained magnetic composite was washed several times with distilled water where the wash water was removed after the application of the magnetic separation process. The magnetic composite was dried at room temperature and was called MZ.

Characterization

The images of scanning electron microscopy (SEM) were obtained using the scanning electron microscope Philips XL-30. X-ray powder diffraction (XRD) analysis was performed on a MINIFLEXIII Desktop X-ray diffractometer, Rigaku, using radiation Cu Kα_1 ($\lambda = 1.5406$ Å) at 30 kV and 15 mA in the range of 2θ from 5° to 80°, with a scan rate of 0.05° per second. Magnetization measurements were obtained at room temperature in magnetic fields up to

20 kOe using a vibrating sample magnetometer (Princeton Applied Research, model 4500). Thermogravimetry analysis (TG) was performed on a Mettler Toledo thermobalance 851 where a quantity of 10 mg of sample was filled into the aluminum plate, and was heated at a heating rate of 10 °C min^{-1} under O_2 atmosphere with a flow rate of 50 cm^3 min^{-1}. Fourier transform infrared (FTIR) spectra of the dispersed samples in KBr pellets were recorded by a Nicolet Nexus 670 FTIR spectrometer.

Performance of MZ as magnetic adsorbent

The efficiency of the magnetic separation and the adsorptive property of MZ were evaluated using batch adsorption tests where a vial containing 50 mg of MZ particles with 5 mL of Reactive Orange 16 (RO16) dye was agitated for 120 min. A Quimis shaker, model Q225 M, at 360 rpm, was used. After agitation, the vial containing the MZ and the solution was placed on the magnet and was left for 60 min for the settling of the particles on the bottom due to the attraction by magnetic field. After that, 4 mL of supernatant solution was carefully removed and transferred into another vial and its absorbance was read at 493 nm by a UV–Visible spectrophotometer, Micronal, model B582. Then, this supernatant was centrifuged for 20 min and a new reading of absorbance was obtained. The adsorption percentage of each step was calculated by Eq. (1) and this study was carried out in triplicate.

$$\text{Adsorption percentage } (\%) = \frac{(\text{initial absorbance} - \text{final absorbance}) \times 100}{\text{initial absorbance}} \quad (1)$$

Results and discussion

Magnetite particles from partial oxidation Fe(II) ions

When aliquots of NaOH are added into a ferrous solution in the total absence of oxidant agent, the OH^- ions bound to Fe(II) ions to form a ferrous hydroxide gel, $Fe(OH)_2$. However, when the Fe(II) ions are from the ferrous sulfate solution and the suspension is aerated by stirring it ensures a progressive partial oxidation of Fe(II) ions to Fe(III) ions such as it was observed in this work. The mixture turned to a dark green color.

The partial oxidation of ferrous ions by the dissolved oxygen in distilled water leads to the formation of mixed ferrous-ferric hydroxides known as green rusts (GR) due to bluish-green colors which are layered structures consisting of alternating positively charged hydroxide layers and hydrated anion layers [25, 26]. GR are commonly prepared in the laboratory by aerial oxidation of $Fe(OH)_2$ precipitates and very seldom prepared by coprecipitation of Fe(II)-Fe(III) solutions [27].

NaOH was added drop by drop into Fe(II) solution in order to verify the pH change during the formation of dark green precipitates. The typical pH titration curve of the ferrous sulfate solution was plotted as a function of added NaOH volume, and is illustrated in Fig. 1. The curve is essentially characterized by one plateau region. With addition of NaOH, a rapid increase of the pH 3.7 of the Fe(II) solution up to pH 7.2 was observed and pratically remains unchanged during the process involving the formation of GR. The plateau was observed beginning at 7.2 and finishing at 8.4. Then, a jump of pH indicated an excess of OH^- ions in the solution.

The plateau was observed until pH 8.4 by addition of 4.50 mL of NaOH into the solution of 0.0065 mol of Fe(II). It corresponded to the addition of 0.0113 ± 0.0001 mol of OH^-, indicating that less than 2 mol of OH^- per mole of Fe(II) was consumed different from formation of the $Fe(OH)_2$ gel. This can suggest the formation of an oxidation final product of other hydroxides as hydroxysulfate green rust attributed to the dark green precipitate cited by Génin and Ruby [27].

After heating for 75 min in a water bath, the dark green precipitate turned to a black, dense, and magnetic precipitate identified as magnetite in the characterization studies.

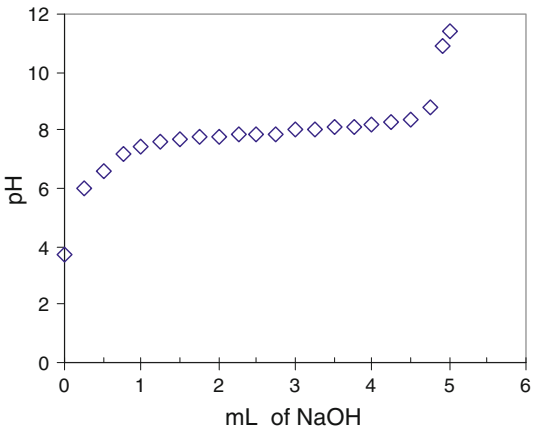

Fig. 1 Evolution of pH curve during titration of the ferrous sulfate solution with a NaOH solution in the aerated mixture

The oxidation of hydroxysulfate green rust to the magnetite, $Fe^{II}Fe_2^{III}O_4$, occurred by heating, in addition to the aerial oxidation and oxidation by SO_4^- ions which were present within reaction medium. Génin et al. [28] related that the GR could not be a precursor of magnetite by a simple aerial oxidation.

For simplicity reasons, the formation reaction of the magnetite from the precipitation and partial air oxidation of Fe(II) ions can be suggested by the Eq. 2. The GR precipitate was produced due to oxidant aqueous medium and aeration. The reaction is completed by heating to the formation of the magnetite. The mechanism of magnetite formation from the intermediate precipitate of GR was not discussed herein due to reaction complexity and necessity to complementary studies.

$$Fe^{II}SO_4 + NaOH + O_2 + H_2O \rightarrow (GR) \rightarrow \text{heating} \rightarrow Fe^{II}Fe_2^{III}O_4 \quad (2)$$

The chemical reactions of formation of the magnetite from precipitation and partial oxidation from Fe(II) ions are easily affected by the quantity of OH^- ions, rate of stirring of the solution, the Fe(II)/OH^- ratio, the heating temperature, and the heating time. All these variables must be carefully controlled, otherwise another iron oxide like reddish-brown rust, α-Fe_2O_3, known as hematite can form.

SEM studies

Figure 2 shows a fine gray powder of the synthesized zeolite SZ. In Fig. 3, the SEM images of SZ, MAG, and MZ revealed non-uniformly sized particles. Clustered particles can be seen. These clusters are irregularly shaped grains of various sizes, usually less than 500 nm. However, some are as big as 1 μm and there is no narrow distribution of particle sizes.

The SZ showed clusters of spherical particles of varying sizes and larger than the particles MAG. The MAG powder is an agglomeration of clusters of different sizes made of tiny particles.

Fig. 2 Synthesized zeolite SZ

The image of the MZ showed particle clusters as MAG. It is observed to be tiny particles, probably of MAG particles, adhered to larger particles, probably SZ, to form the magnetic zeolite MZ. The origin of the clusters can be ascribed to the used drying process for obtaining of powdered samples. Drying process caused the formation of clustered particles. The MAG and MZ images showed smaller clusters and larger clusters having sizes 100 nm or greater.

Magnetization measurements

The particle morphology and distribution of particle sizes can affect the magnetic properties of a material such as residual magnetism. The black powder MAG exhibited a strong magnetic attraction with the approach of a magnet, as shown in Fig. 4, and with the withdrawal of the magnet, any residual magnetism was not observed. The MZ also exhibited a strong magnetic attraction in the presence of a magnet, as intense as MAG particles (Fig. 4).

The magnetic properties of the composts MAG and MZ were evaluated using a vibrating sample magnetometer.

The two powdered samples were subjected to magnetic measurements at 300 K by the field cycling between ±20 kOe and their magnetic properties were investigated on the obtained hysteresis loops shown in Fig. 5. The values of the saturation magnetizations (*M*s), coercivities (*H*c), and remanence or remanent magnetizations (*M*r) are summarized in Table 1.

A saturation magnetization (*M*s) value of the MAG nanoparticles equal to 72.6 emu g^{-1} was found which is a high value but significantly lower than the value for bulk size of the magnetite (92 emu g^{-1}) [29]. This significant decrease in the Ms value can be attributed to the nanosize dimensions of the particles and to the effects of anisotropy and oxidation of the surface and shape of non-spherical samples.

For the MZ, a *M*s value lower than that of MAG was observed. The decrease is attributed to the effects of dispersion of non-magnetic volume of SZ phase in the composite MZ. The decreasing is proportional to the 1:3 MAG/SZ ratio used in the synthesis.

The insert in Fig. 5 illustrates the hysteresis loops in the field cycling between ±5 kOe. Both MAG and MZ samples showed low values of coercivity (*H*c) and remanence (*M*r).

A value of *H*c indicates that there is a magnetic storage in the sample; therefore, hysteresis was observed. This means that the samples did not behave purely super paramagnetically even though the particle size was very small. The coercivity is affected by particle size. The coercive field increases with the average size of the particles. As can be seen in the SEM images (Fig. 3), the samples are formed by the clustered particles, so the result of the

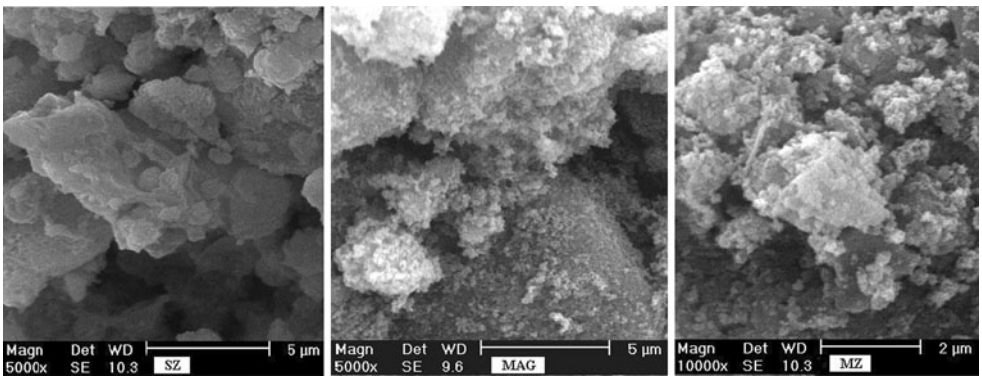

Fig. 3 SEM images of magnetite MAG, synthetic zeolite SZ, and magnetic zeolite MZ

Fig. 4 Magnetic responses of the MAG (*left*) and MZ (*right*) in contact with a magnet

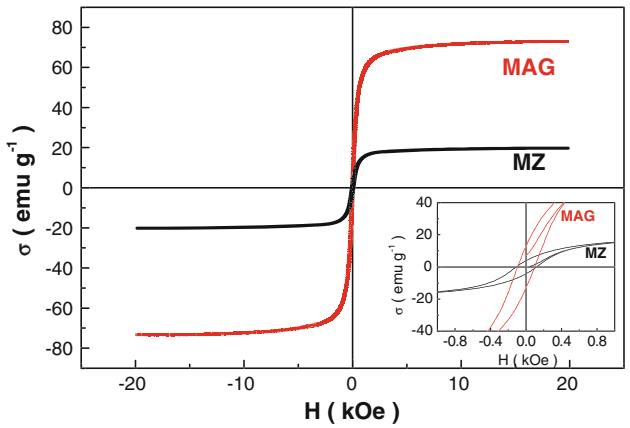

Fig. 5 Magnetization loops measured at 300 K for the particles of MAG and MZ

magnetic properties represents a total for all particles present in the clusters. The magnetic properties can also be influenced by the growth of the clusters. The non-zero coercivity can be explained because the magnetic properties were more affected by the cluster growth than by the reduction process and the formation of very fine particles. The clustering of the small particles in the sample could be responsible for the deviations from magnetic measurements.

Table 1 Magnetic properties of MAG and MZ at 300 K

Samples	*M*s (emu g^{-1})	Hc (Oe)	*M*r (emu g^{-1})
MAG	72.6	−0.09; +0.1	−12.1; +11.7
MZ	19.9	−0.1; +0.1	−4.1; +4.1

A low value of remanence, *M*r, as showed by the samples means lower value of the residual magnetization.

In practice, these magnetic properties described favorable condition for the use of magnetic separation technique. The particles of magnetic adsorbent can be removed from the liquid by applying an external magnetic field and resuspended in another liquid medium after removal of the external magnetic field.

X-ray diffraction

XRD patterns of the three types of samples are shown in Fig. 6. It can be seen that the peaks in the synthesized magnetite MAG, Fe_3O_4, are in agreement with the data of the face-centered cubic of the reported pattern of reference magnetite in the ICDD n° 19-629. All MAG peaks showed broad diffraction lines and well-defined peaks indicating that the crystallites were very small.

The obtained zeolite from coal fly ash (SZ) showed crystalline components with no peaks of magnetite indicating its absence in accordance with the composition of the material. The peaks are assigned to the hydroxy sodalite (ICDD 00-011-0401) as the zeolitic phase mixed with quartz (SiO_2) and mullite ($2SiO_2{\cdot}3Al_2O_3$ or $Al_6Si_2O_{13}$) and some metals remaining in the sample after the heat alkaline treatment of the coal fly ash. The hydroxy sodalite is represented by the chemical formula $Na_4Al_3Si_3O_{12}(OH)$.

For XRD pattern of the MZ, the illustrated peaks were related to the peaks found for MAG and SZ.

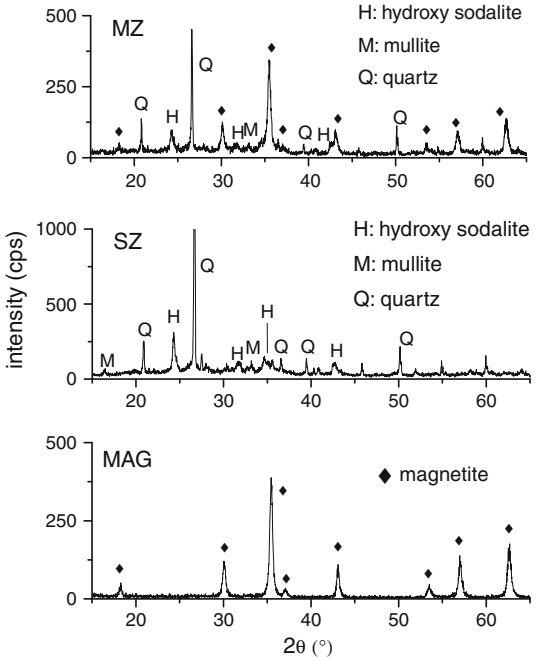

Fig. 6 X-ray diffraction patterns of the MAG compared with SZ and MZ

For better comparison, the values of 2θ of the observed peaks in the MAG and MZ were indicated in Table 2 together with the values of 2θ angle related to the relative intensity and the diffraction plane (*hkl*) of the reference standard of magnetite.

The crystallite size (D) of magnetite particles for samples of MAG and MZ was estimated from the X-ray diffraction peak (311) using the Scherrer formula [30] represented by the Eq. 3. The Scherrer equation is limited to nano-scale and is given for particles of spherical shape (shape factor of typical value 0.9). In this work in order to apply the Scherrer formula the spherical shape of nanoparticles was considered. The estimated crystallite sizes of magnetite of the samples are given in Table 3. As can be seen the crystallite is in nanosize, which may be smaller or equal to the grain size. The nanoparticles were also evidenced in the XRD pattern by broad and distinct peaks.

$$D = \frac{0.9\lambda}{\beta_{1/2}\cos\theta} \quad (3)$$

Table 3 XRD crystallite size of the MAG and MZ for the (311) peak of magnetite

Sample	MAG	MZ
Crystallite size (nm)	17	18

where λ is the wavelength of the X-ray source ($Cu_{K\alpha 1}$), $\beta_{1/2}$ is the angular width at the half maximum intensity of the diffraction peak (rad), and θ is the Bragg angle.

FTIR analysis

The FTIR spectra of the materials are given in Fig. 7. For MAG it was possible to visualize the sharp and strong absorption band at 568 cm^{-1} attributed to the Fe–O bond of magnetite. No absorption band at 632 cm^{-1} was observed as in the magnetite from coprecipitation of Fe(II) and Fe(III) ions [31].

A broad absorption band was seen in the region from 4000 to 800 cm^{-1} and clearly showed the overlapping of some vibration modes. This overlapping can be assigned to different O–H stretching modes in H_2O and to the presence of the hydroxyl groups on magnetite particle surfaces as Fe–OH. It may also be attributed to the very strong hydrogen bonds in magnetite particles.

When exposed to free water molecules from aqueous solutions, the surfaces of metal oxide such as the magnetite particles undergo surface hydroxylation and hydration. Many hydroxyl groups and hydrogen bonds and absorbed water molecules on the surface of the magnetite particles are not eliminated during the drying process at room temperature in which the magnetite particles were subjected.

The FTIR spectrum of the SZ was investigated by a comparison with the main absorption bands of sodalite structure that have been reported in the literature [32–34]. The absorption bands that occur at 992, 722, 697, 660, 459, and 429 cm^{-1} were characterized as the infrared absorption bands of the hydroxy sodalite. The broad band at 992 cm^{-1} arises from the asymmetric stretch, ν_{as}(T-O-T, T=Si, Al) located in the 1200–900 cm^{-1} region. The three bands located in the 750–650 cm^{-1} region were attributed to the symmetric stretch ν_s(T-O-T). The bands at 459 and

Table 2 XRD peaks of the (ICDD 19-629) reference magnetite, MAG and MZ

Plane (*hkl*)	311	440	511	220	400	422
Reference peak (2θ)	35.42°	62.51°	56.94°	30.10°	43.05°	53.39°
Relative intensity reference peak	100	40	30	30	20	10
Peak (2θ) in the MAG and MZ	35.5°	62.8°	57.3°	30.3°	43.3°	53.6°

Incident X-ray Cu Kα

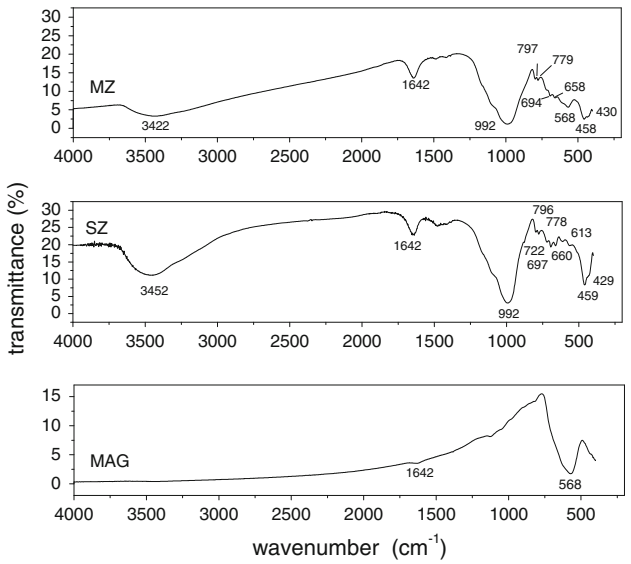

Fig. 7 The FTIR spectra of MAG, SZ, and MZ

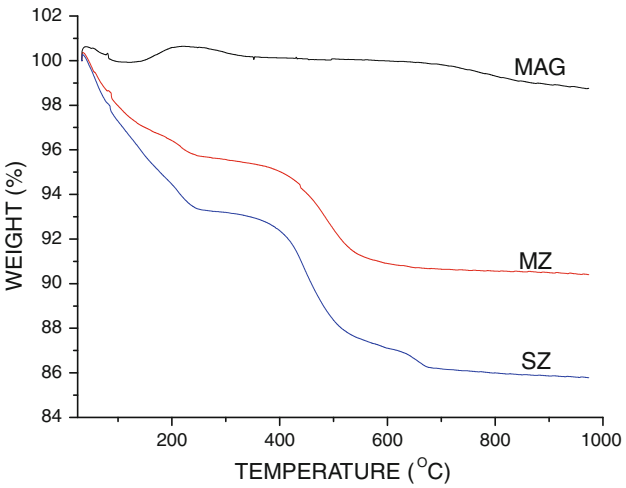

Fig. 8 Thermograms of MAG, SZ, and MZ under O_2 atmosphere

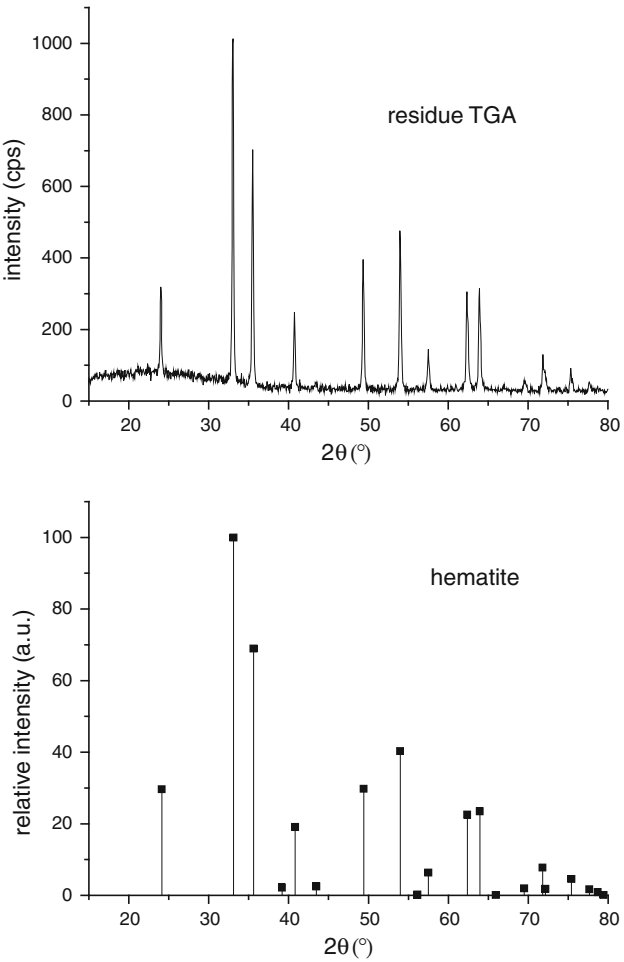

Fig. 9 X-ray diffraction patterns of the residue TGA from the MAG and of the reference hematite in the ICDD n° 010890598

429 cm^{-1}, in the range 500–420 cm^{-1}, were assigned to the bending vibration of δ(O-T-O). Absorption bands around 796, 778, and 613 cm^{-1} can be due to the combination modes and overlap of (Al, SiO_4) and Si–OH vibrations of the hydroxylated quartz [35, 36] in the SZ. The broad band at about 3400 cm^{-1} and a band at 1642 cm^{-1} band were attributed to water of hydration in the zeolitic sample.

The FTIR spectrum of the MZ illustrates the overlapping of the absorption bands of the synthesized zeolite (75 %) and magnetite (25 %) particles in the region from 750 to 500 cm^{-1}. The appearance of a well-defined band of the Fe–O vibrations of the MAG particles can be seen at 568 cm^{-1}. Comparing the spectra and considering the sample containing 25 % of MAG particles, the intensity of the strong and broad absorption band in the region from 1600 to 1250 cm^{-1} decreased, probably indicating the possible formation of electrostatic forces and hydrogen bonding between SZ and MAG particles with hydroxyl groups, to form the magnetic composite.

TG analysis

Figure 8 shows the thermograms of mass variation with increasing temperature under O_2 atmosphere where the structure differences of the materials MAG, SZ, and MZ can be observed.

In the thermogram of the MAG, a small mass loss was observed in the temperature range from 25 to 974 °C. A final product of brown color having no magnetic properties with 98.8 % of the initial mass was obtained. The analysis of the final product by XRD, Fig. 9, indicated that it was a hematite. The phenomenon which might have occurred with increasing temperature under O_2 atmosphere may be

the oxidation of magnetite to maghemite to be transformed to the thermodynamically stable hematite, α-Fe_2O_3.

The thermogram of the SZ showed significant mass loss with increasing temperature and described change in chemical structure of the synthetic zeolite until reaching a stable product containing 85.8 % of the original mass at temperature of 974 °C.

The thermogram of the MZ, which is a composite assigned by one part of MAG and three parts of SZ, also showed a significant mass loss but less than SZ. A non-magnetic solid of 90.4 % of the initial mass was observed as a final product. This percentage value found is according to the MZ composition in the prepared ratio of one MAG and three SZ proving the formation of the composite MZ.

Effectiveness of magnetic separation performance of MZ

The particles of MZ exhibited magnetism in magnetic field from the magnet-forming agglomerates that settle rapidly at bottom of the vial by magnetic forces. Figure 10 shows that the suspended particles in the liquid medium were immediately attracted and agglomerated by a magnet easily allowing the solid–liquid separation. This step is required in the final processes of wastewater treatment. After the magnet removal, the particles were dispersed, again, in the liquid phase, enabling to apply the following desorption technique and the reuse.

According to the described procedure, the magnetic separation performance of MZ was evaluated. After 120 min of agitation, the supernatant was cloudy due to the suspension and dispersibility of the dark MZ particles. So the vial was left on the magnet for 60 min. After that, the supernatant was clear without the MZ particle suspension, and the RO16 absorbance was read. All MZ particles were settled at the bottom of the vial. After that, the same supernatant was subjected to a centrifugation for 20 min at 3000 rpm, and a new absorbance was read.

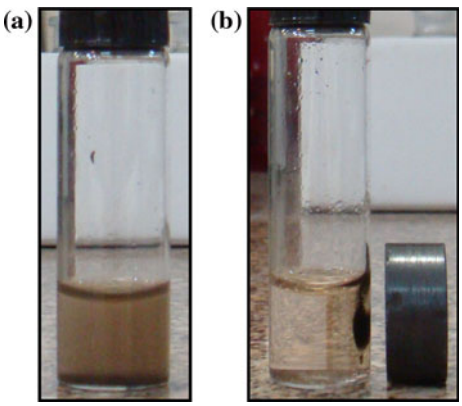

Fig. 10 Application of magnetic separation technique: **a** Vial with a suspension of MZ particles in the solution of dye Reactive Orange 16, **b** Vial with the MZ particles in the solution dye Reactive Orange 16 being attracted by the magnet after 5 s

Table 4 Values of adsorption percentage of RO16 dye on the MZ

Separation technique	Adsorption (%)
Magnet (60 min)[a]	90 ± 3
Magnet (60 min) + centrifugation (20 min)[b]	90 ± 3

[a] The vial containing MZ and supernatant was placed on a magnet for 60 min

[b] The separated supernatant by a magnet was centrifugated for 20 min

The results of the Table 4 indicated the magnetic separation to be as efficient as centrifugation, since no difference was found between the absorbance values. The RO16 recovery from the read absorbances was 90 % in both techniques. Therefore, the effectiveness of the MZ as an adsorbent for the RO16 dye and the high performance of the application of magnetic separation was confirmed. The results also confirm a good binding between the magnetite and the zeolite, since no additional drop in the absorbance was observed after centrifugation. A complete study of adsorption was presented by Fungaro et al. [24].

The time of 60 min that the vial stayed on the magnet was sufficient to override a centrifugation of 20 min. It is noteworthy that the established time of 60 min can be much reduced using a stronger magnetic field. The settling time of magnetic particles depends on the force of the applied magnetic field. On the stronger field gradient, the rate of settling increases, and, therefore, the separation time can be significantly reduced.

Conclusions

Magnetite was preferentially formed by heating of a GR suspension in aqueous medium containing dissolved oxygen by aerial process and sulfate ions at pH higher than 11. The GR precursor of magnetite was easily obtained by precipitation and partial oxidation of Fe(II) ions but the variables must be carefully controlled.

This magnetite combined with zeolite from the coal ash, an abundant industrial waste, produced a magnetic adsorbent which exhibited magnetic properties by being easily attracted and separated from the aqueous solutions using a magnet.

The performance of the magnetic adsorbent applied for magnetic separation technique was comparable to the centrifugation process. The results showed that the Reactive Orange 16 dye was favorably adsorbed on the magnetic adsorbent MZ from aqueous solution, indicating a

potential application as an alternative and sustainable technology for wastewater treatment.

Acknowledgements Thanks to the National Council for Scientific and Technological Development (CNPq), Brazil, for financial support and to the Carbonífera do Cambuí Ltda, PR, Brazil, for supplying coal ash samples.

References

1. Ambashta RD, Sillanpää M (2010) J Hazard Mater 180:38
2. Liua H, Qinga B, Yea X, Li Q, Leec K, Wu Z (2009) Chem Eng J 151:235
3. Yamamura APG, Yamaura M, Costa CH (2011) Int J Nucl Energy Sci Technol 6:8
4. Tamai H, Nakamori M, Nishikawa M, Shiono T (2011) Mater Sci Appl 2:49
5. Feng D, Aldrich C, Tan H (2000) Hydrometallurgy 56:359
6. Misaelides P (2011) Microporous Mesoporous Mater 144:15
7. Wang S, Peng Y (2010) Chem Eng J 156:11
8. Oliveira LCA, Petkowiczb DI, Smaniottob A, Pergher SBC (2004) Water Res 38:3699
9. Nah IW, Hwang K-Y, Shul Y-G (2007) Powder Technol 177:99
10. J-l Cao, Liu X-W, Fu R, Tan Z-y (2008) Sep Purif Technol 63:92
11. Barquist K, Larsen SC (2010) Microporous Mesoporous Mater 130:197
12. Pandeya VC, Singha JS, Singha RP, Singhb N, Yunus M (2011) Resour Conservation Recycl 55:819
13. Dutta BK, Khanra S, Mallick D (2009) Fuel 88:1314
14. Siddique R (2010) Resour Conservation Recycl 54:1060
15. Chugh Y, Patwardhan A, Munish S, Botha F (2006) Fuel 85:2323
16. Van de Lindt JW, Carraro JAH, Heyliger PR, Choi C (2008) Resour Conservation Recycl 52:1235
17. Basu M, Pande M, Bhadoria PBS, Mahapatra SC (2009) Prog Nat Sci 19:1173
18. Belviso C, Cavalcante F, Fiore S (2010) Waste Manage 30:839
19. Querol X, Moreno N, Umaña JC, Alastuey A, Hernández E, López-Soler A, Plana F (2002) Int J Coal Geol 50:413
20. Ríos CA, Williams CD (2008) Fuel 87:2482
21. Carvalho TEM, Fungaro DA, Magdalena CP, Cunico P (2011) J Radioanal Nucl Chem 289:617
22. Chunfeng W, Jiansheng L, Xia S, Lianjun W, Xiuyun S (2009) J Environ Sci 21:127
23. Jamil TS, Ibrahim HS, Abd El-Maksoud IH, El-Wakeel ST (2010) Desalination 258:34
24. Fungaro DA, Yamaura M, Carvalho TEM (2011) J At Mol Sci 2:305
25. Sergent A-S, Jorand F, Hanna K (2011) Chem Geol 289:86
26. Refait Ph, Géhin A, Abdelmoula M, Génin J-MR (2003) Corros Sci 45:659
27. Génin J-MR, Ruby C (2004) Solid State Sci 6:705
28. Génin J-MR, Ruby C, Géhin A, Refait Ph (2006) Geoscience 338:433
29. Cullity BD, Graham CD (2009) Introduction to magnetic materials, 2nd edn. IEEE Press, New Jersey
30. Cullity BD (1972) Elements of X-rays diffraction, 2nd edn. Addison-Wesley Publishing Company, Massachusetts
31. Yamaura M, Camilo RL, Sampaio LC, Macedo MA, Nakamura M, Toma HE (2004) J Magn Magn Mater 279:210
32. Yao J, Wang H, Ratinac KR, Ringer SP (2006) Chem Mater 18:1394
33. Alkan M, Hopa C, Yilmaz Z, Güler H (2005) Microporous Mesoporous Mater 86:176
34. Johnson GM, Weller MT (1997) Stud Surf Sci Catal 105:269
35. Abdrakhimova ES, Abdrakhimov VZ (2007) Russ J Inorg Chem 52:345
36. Jutarosaga T, Jeoung JS, Seraphin S (2005) Thin Solid Films 476:303